# The Soap Opera of Metal Catalysis in Epoxy-Acid Vitrimers

Diego Ciardi, Ianis Retailleau, François Tournilhac

# The Soap Opera of Metal Catalysis in Epoxy-Acid Vitrimers

Diego Ciardi[‡a], Ianis Retailleau[‡a,b], François Tournilhac[a]*

[a]Molecular, Macromolecular Chemistry, and Materials, ESPCI Paris, PSL University, CNRS, 10 rue Vauquelin, Paris 75005, France.

[b]Univ. Grenoble Alpes, CEA, Liten, Campus Ines, 73375 Le Bourget du Lac, France

Author information

Corresponding author. François Tournilhac. francois.tournilhac@espci.fr.

orcid.org/0000-0002-6775-1584

Author. Diego Ciardi.[‡] orcid.org/0000-0001-7303-8569

Author. Ianis Retailleau.[‡] orcid.org/0009-0001-6558-425X

[‡] authors contributed equally.

Key words: metals soaps, transesterification, vitrimers

**Abstract:** Precipitation of bivalent metal carboxylates is a well-known issue in detergency, resulting in decreased efficiency and unwanted accumulation of lime soap on laundry. We demonstrate that the same phenomenon is occurring in formulations of metal-catalyzed epoxy-acid vitrimers. When for instance a Zn (II) salt and glutaric acid are allowed to meet each other in the same reaction feedstock, precipitation takes place, resulting in phase-separation of zinc glutarate and glutarate-poor polymer network, showing no vitrimer properties. We present a strategy to overcome this issue based on step addition at a single end of the dicarboxylic acid monomer, prior to contact with zinc. In this case, formation of crystalline zinc soap is completely avoided, and the network shows thermo-stimulated stress relaxation. This strategy is particularly appealing for the synthesis of polyhydroxyester networks showing high-$T_g$ and fast relaxation.

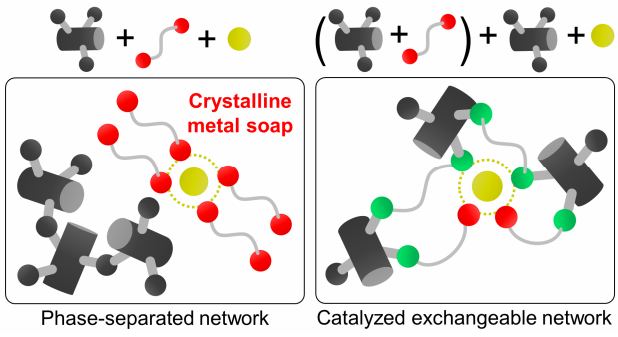


Table of content illustration.

## INTRODUCTION

Vitrimers are polymer networks with thermally exchangeable links, which enable them to flow when heated while remaining essentially insoluble, even in a good non-reactive solvent where they swell without dissolving.[1] Thus, contrary to conventional polymer networks, vitrimers exhibit a finite relaxation time and retain reprocessability and recyclability after crosslinking. A catalyst is often present, to increase the rate of exchange, leading to shorter relaxation times.[2]

In polyhydroxyester vitrimers, the exchange reaction is transesterification, and various catalysts such as Zn, Sn, N and P compounds,[3,4,5,6,7,8,7,9] or enzymes,[10] have been proposed to increase the exchange rate. Zn(II)-based catalysts are most often considered. They show high thermal stability and also catalyse the epoxy-acid addition,[11] a useful reaction to produce β-hydroxylester exchangeable links, thereby reducing the curing time and occurrence of secondary reactions. To prepare metal-catalyzed polyhydroxyester networks, an epoxy resin is typically mixed with a fatty acid whose carboxylic functions have been neutralized with Zn(II) ions. This step creates Zn(II)-carboxylate complexes, which are essential both for the epoxy-acid addition reaction and for catalysis of the subsequent transesterification process responsible of vitrimeric behavior.

Based on IR and X-ray absorption spectroscopy, Demongeot et al.,[12] suggested that, upon reaction of Zn(II)-carboxylate with an epoxy group, the Zn(II) ion becomes coordinated with ester and alkoxide ligands (Figure 1a). Thus, the metal plays a double role of reapproaching the reactants (Figure 1b) and activating the C=O bond by electron withdrawing effect thereby reducing the transesterification energy barrier.

Such transition between the two coordination spheres is therefore necessary for both the epoxy-acid addition and transesterification to be catalyzed. Hence, formation of a metal carboxylate constitutes the first step in the formulation of epoxy-acid vitrimers and maintaining its solubility in the reaction medium is a necessary condition to perform the homogeneous catalytic cycle.

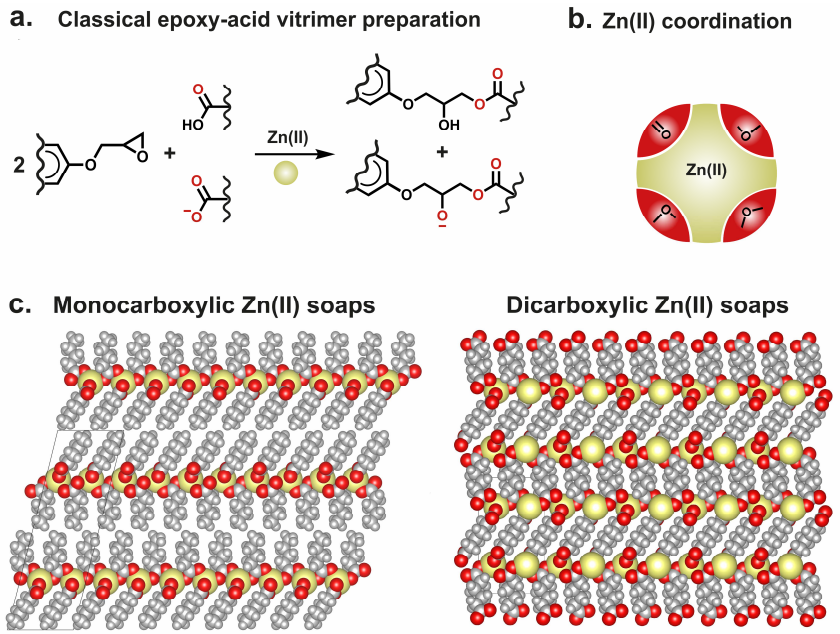


**Figure 1:** (a) main reaction in epoxy-acid vitrimers, with the formation of β-hydroxylester and β-oxyester links upon epoxy-acid and epoxy-carboxylate addition, respectively. Red atoms highlight the possible coordination sites of Zn(II); (b) coordination sphere of Zn(II) in the final vitrimer network suggested by Demongeot et al.[12] (c) crystalline structure of a linear monocarboxylate (zinc pentanoate)[13] and dicarboxylate (zinc adipate)[14] soaps (see Table S1 for crystallographic details).

In detergency, long chain carboxylates such as oleate, stearate or laurate have tendency to precipitate Ca(II) and Mg(II) ions in water.[15] This primarily occurs in hard water, where the concentration of divalent ions is higher, resulting in the waste of active material and undesirable aggregation of soap scum on laundry. These so-called metal soaps are also observed in other contexts. They are used as additives to coatings,[16,17] lubricating agents, fillers[18] and heat stabilizers in plastics,[19] or in the synthesis of nanoparticles.[20] They are also found in oil paintings as degradation products.[21,22] As regards metal catalysis, it was experienced that metal soaps precipitation reduces transesterification reaction yield in the production of biodiesel from fatty acids.[23]

The structure of metal soaps has been studied using X-ray, DSC and IR spectroscopy.[16,24,25,26,27,28] When cations are coordinated by a saturated linear-chain monocarboxylic acid, the resulting soaps are crystalline solids. The crystal structure often shows 2D networks of metal ions, connected by carboxylate bridging ligands (Figure 1c).

In the case of linear-chain dicarboxylic acids, both terminals can coordinate a metal ion, thereby producing a three-dimensional polymeric crystal structure, also called metal-organic

framework.[29,30,31,32] These species generally exhibit higher melting points compared to the corresponding dicarboxylic acid or monocarboxylate soap. As practical example, succinic acid melts at 184°C and zinc butanoate around 160°C but zinc succinate is stable and degrades starting from ~450°C without undergoing any transition.[32]

In terms of vitrimer formulations, these thermal properties could have significant implications on their achievement. We hypothesize that the energy required to melt the metal soap adds a barrier to dissolving the catalyst inside the reaction medium, thereby hindering the homogeneous catalytic activity in the final network. Indeed, at the moment, the majority of publications concerning metal-catalyzed epoxy-acid vitrimers focus on the use of branched carboxylic acids alongside with Zn(II)[1,2,12,33,34,35,36,37,38] which should avoid the formation of high-melting point metal soaps. However, relying on branched carboxylic acids limits the selection to a narrow range of available starting materials, resulting in products with glass transition temperature between -20°C and +30°C. This range make them poorly suitable for use as either elastomers or thermosets. Higher $T_g$ and denser networks are typically obtained using anhydrides as curing agents.[1] Nonetheless, in anhydride-based vitrimers, the formation of hydroxyl groups – essential for the transesterification reaction – is limited, and an enrichment of the network might be desirable to increase stress-relaxation rate.[39] Systems based on linear − or more generally rigid − dicarboxylic acids were shown to attain higher $T_g$, but these typically rely on other catalytic approaches, such as organic[3,6,40] or enzymatic catalysis[10], which may result in more temperature-sensitive systems. The scarcity of studies combining metal catalysis with rigid dicarboxylic acids[41,42] supports our hypothesis of a potential incompatibility between the two in acid-epoxy vitrimers. In a perspective of broadening the scope of metal catalysts, we investigate the role of the carboxylic acid/metal pair (metal soap) in the preparation of epoxy-acid vitrimers. Upon analyzing the conditions that lead to catalyst crystallization, we developed a synthetic strategy for creating high-$T_g$ acid-epoxy vitrimers where metal catalysis is effectively integrated into the network, thereby enhancing relaxation properties.

## EXPERIMENTAL SECTION

**Chemicals.** *Epoxy resins:* poly[(phenylglycidyl ether)-co-formaldehyde] (PPGEF, epoxy equivalent weight EEW = 177g/mol) was graciously provided by Huntsman (Epalloy 8330 grade); 1,4-cyclohexanedimethanol diglycidyl ether (CHDE) was bought from Biosynth.

*Diacids:* the fatty acid derivative (FatA) was provided by Croda (Pripol 1009 grade, acid equivalent weight AEW = 285 g/mol). Glutaric acid (GluA) was bought from Abcr, undecanedioic acid (UDA) and cis-1,4-cyclohexanedicarboxylic acid (CHDA) from TCI, homophtalic acid (HomA) from Sigma-Aldrich. *Metal salts and organotin:* zinc acetate ($Zn(OAc)_2$), lithium acetate (LiOAc) and cesium carbonate ($Cs_2CO_3$) were bought from Alfa Aesar, zinc acetylacetonate ($Zn(acac)_2$) and tin acetate ($Sn(OAc)_2$) from Sigma-Aldrich and butyl stannoic acid (or monobutyl tin oxide hydroxide, BuSnOOH) from TCI.

**Nuclear magnetic resonance (NMR) spectroscopy.** $^{1}H$ NMR and $^{13}C$ NMR spectra were recorded at 24°C in DMSO-$d_6$ using a Bruker AVANCE400 spectrometer. Chemical shifts were referenced using the residual solvent peaks.

**Infrared spectroscopy analysis.** IR measurements were carried out using a Bruker TENSOR 37 spectrometer equipped with a Specac golden gate attenuated total reflection (ATR) heating cell. IR kinetics were monitored at 145°C.

**Size Exclusion Chromatography (SEC).** PPGEF and BranchA were dissolved in THF at a 1 $mg \cdot mL^{-1}$ concentration and toluene was added as internal standard. All solutions were filtered through 0.2 µm PTFE filters before injection. SEC was performed on a Viscotek GPCmax/VE2001 with THF as elution solvent and chromatograms were recorded with a TDA 305 triple detection array. The solvent flow rate was set to 1.0 $mL \cdot min^{-1}$ and injection volumes were of 100 µL. The toluene peak of all samples was set to the same retention time. To compare the chromatograms, the data was normalized by their respective maxima.

**Differential scanning calorimetry (DSC).** DSC measurements were performed at a heating and cooling rate of 10°C/min under helium using a TA DSC 250 analyzer. An initial heating ramp was carried out between 0°C and 200°C, and the temperature was subsequently returned to 0°C. A second heating ramp was then performed from 0°C to 200°C.

**Microscopy.** Polarized optical microscopy observations were made on a Leica DMRXE microscope equipped with a Fluotar 5 × 0.12 objective, a Sony XCD-100CR digital camera and a Linkam LTS350 heating stage. Mixtures were placed between a glass slide and coverslip for temperature investigations between 30 and 200 °C.

**Swelling Tests.** Swelling tests were carried out in a round bottom flask, using ~0.25 g of sample in THF, at 85°C under reflux for 24h. The swollen samples were subsequently weighed and dried under vacuum at 75°C, for 5h. The dried samples were weighed and the swelling ratio $Q$ was obtained according to the equation: $Q = 100 \cdot (m_s - m_d) / m_d$, where $m_s$ and $m_d$ are the mass of the swollen and dried samples, respectively.

**Powder X-Ray diffraction (XRD).** Powder X-ray diffraction data were measured at room temperature with a Bruker D8 Advance diffractometer (Cu Kα radiation, λ = 1.54 Å) in the Debye−Scherrer geometry (transmission mode) using a Linxeye detector. Crystallite dimensions were obtained using the Scherrer equation (see SI).

**Synchrotron-sourced X-Ray Scattering.** X-ray scattering measurements were conducted at beamline SWING at SOLEIL (Saint-Aubin, France) at 12 keV (SAXS) or 16 keV (WAXS) energy using 1-3 mm thick self standing films with a sample to detector distance of 6 m (SAXS) or 0.5 m (WAXS). The 2D SAXS patterns were integrated (Foxtrot 3.5.10 software) and normalized with an $H_2O$ standard to create 1D intensity ($cm^{-1}$) versus wavevector $q$ ($Å^{-1}$) patterns. 1D traces were fitted with SasView 6.0.[43]

**Rheological measurements.** Rheological measurements were performed using an Anton Paar 702 rheometer in the torsional or parallel plate geometry, depending on the nature of the sample investigated. For torsional geometry, the dimension of the specimen was 45×10×4 $mm^3$ and the normal force was set at -1 N before every experiment, to keep the sample under constant tension. For PPGEF/FatA/Zn(II), the reactive mixture was sandwitched between Ø = 25mm parallel plates and cured inside the rheometer. Stress-relaxation were subsequently recorded. Stress-relaxation experiments were carried out between 160°C and 180°C, by applying a shear strain of 1% for samples in torsion, while 0.3% in parallel plate. Before every experiment, an equilibration time of 10 min at the desired temperature is programmed. The normalized relaxation modulus *G(t)* is fitted with a stretched-exponential function and an average relaxation time $\langle\tau\rangle$ at each temperature is extracted, according to the equations:

$$G(t) = G_\infty + G_0 e^{-(t/\tau^*)^\beta} \qquad \langle\tau\rangle = \frac{\tau^*}{\beta}\Gamma\left(\frac{1}{\beta}\right)$$

where $G_\infty$ is the residual stress obtained from the fitting model, $G_0$ is the pre-exponential factor, $\tau^*$ the relaxation time, $\beta$ the relaxation exponent and Γ the gamma function. The values of $G_\infty$, $\langle\tau\rangle$ and $\beta$ are reported in Table S4. An activation energy $E_a$ is then extracted from the plot of $\ln\langle\tau\rangle$ against $1/T$. Amplitude sweep measurements at room temperature were carried out on vitrimer networks between 0.01 and 1% shear strain at 1 rad/s, followed by temperature sweep measurements at 1 rad/s between 30°C and 180°C, using a 0.05% imposed shear strain.

**Metal soaps preparation.** As general procedure, for GluA, UDA, CHDA, HomA-based metal soaps: 1 g of carboxylic acid was mixed with different amounts of a metal salts (from 0.05 to 1 $M^{n+}$ eq. per COOH) into a vial at 180°C for 30 min and mixing the powder we the

aid of a spatula. Typically, the mixture presented in Figure 2 was obtained with 1 g of GluA and 0.34 g of Zn(OAc). For FatA-based metal soaps, 0.1 eq. of $Zn(OAc)_2 \cdot 2H_2O$ were added to FatA (300 g) in a round bottom flask at 100°C, under magnetic stirring. The temperature was gently raised to 180°C and the reaction was conducted under vacuum to remove the produced acetic acid. The obtained metal soaps were analysed by powder X-ray diffraction (powder XRD), DSC and IR.

**Preparation and curing of model epoxy-acid reactive mixtures.** Typical procedure for linear carboxylic acids: the epoxy resin CHDE (5 g) and the carboxylic acid (molar ratio: COOH/epoxy = 1) were mixed at 100°C under manual stirring in a PTFE beaker, until homogenization of the mixture (~ 5 min mixing). The catalyst was added (molar ratio catalyst/epoxy = 0.1), and mixing was kept for another 10 minutes at the same temperature. The resulting mixtures were used for IR and rheological monitoring.

Procedure for the branched carboxylic acid FatA is based on reference 12. The zinc catalyst precursor (zinc acetate) was added to FatA with a molar ratio of Zn(II)/COOH = 0.1. The mixture was gradually heated to 180 °C to perform the ligand exchange and then cooled at room temperature. The epoxy resin is mixed with the precursor (molar ratio acyl/epoxy = 1) at 100°C for 15 mn before IR and rheological monitoring experiments.

**Synthesis of the branched carboxylic acid, BranchA from PPGEF.** In a Teflon beaker, the epoxy resin PPGEF (15 g, 1 epoxy eq.) was reacted with an excess of GluA (4 COOH eq.) and imidazole (IM) as catalyst (0.05 eq.), at 100°C. The excess of carboxylic functions is necessary to ensure the formation of the product BranchA, without incurring in gelation (otherwise observed with only 2 COOH eq.). After 2h, the whole mixture was dissolved in THF. The product was precipitated in water and isolated as a non-tacky waxy solid after vacuum drying 12h at 25°C, then 2h at 90°C.

**Preparation of novolac epoxy-acid networks.** The reactive mixtures are prepared as above, poured into a PTFE mold preheated at 100°C, degassed at 100°C and cured for 16h at 145°C. Rectangular bars for solid rheology were cut from cured samples using a diamond saw. The nomenclature used is:

**PPGEF/GluA**: PPGEF (1 epoxy eq.), GluA (1 COOH eq.), no catalyst.

**PPGEF/GluA/Zn(II)**: PPGEF (1 epoxy eq.), GluA (1 COOH eq.), $Zn(acac)_2$ (0.1 eq.)

**PPGEF/FatA/Zn(II)**: PPGEF (1 epoxy eq.), FatA (1 COOH eq.), $Zn(OAc)_2$ (0.1 eq.)

**PPGEF/BranchA/Zn(II)**: PPGEF (1 epoxy eq.), BranchA (1 COOH eq.), $Zn(acac)_2$ (0.1 eq.)

**PPGEF/BranchA/BuSnOOH**: PPGEF (1 epoxy eq.), BranchA (1 COOH eq.), BuSnOOH (0.05 eq.)

## RESULTS AND DISCUSSION

**Evidence of Metal /carboxylic interaction.** To elucidate the formation of dicarboxylate metal soaps, a series of samples containing glutaric acid (GluA) and various $Zn(OAc)_2$ concentrations were prepared and analysed by DSC. Although metal soaps have high melting points (>300°C), not easily detectable by DSC, the dicarboxylic acid / metal salt interaction is indirectly revealed by the disappearance of the initial melting peaks. The thermograms of different compositions with increasing metal/COOH ratios are shown in Figure S1. The area of the melting endotherm of GluA gradually diminishes as a function of the $Zn(OAc)_2$ concentration, until no melting transition is observed, when the Zn(II)/COOH ratio reaches 0.5. A similar trend was observed when employing different dicarboxylic acids, such as cis-1,4-cyclohexane dicarboxylic, homophthalic and undecanedioic acid, and/or different metal salts, such as LiOAc, $Cs_2CO_3$, $Sn(OAc)_2$ and $Zn(acac)_2$ (Scheme S1). For monovalent cation as $Li^+$ and $Cs^+$, the melting peak of GluA disappears at metal/COOH ratio of 1, consistent with the formation of the monovalent metal glutarate soap.

Precipitation of a new crystalline substance is however well detected through polarizing optical microscopy (POM). Figure 2a shows the thermal cycle of three different GluA-based samples using Zn/COOH molar ratios of 0, 0.1 and 1 (the ratio 0.1 is a typical choice for vitrimer preparation). When no Zn(II) is present, large crystalline domains of ≈100 µm in size are observed, which melted and recrystallized reversibly upon crossing the melting point of GluA (about 98°C). In the case of the composition with 10 mol% of zinc (R = 0.1), small birefringent spots of <10 µm in size appeared during the first heating and remained visible up to 200°C and during all further cycles, regardless the temperature and physical state of the surrounding medium. This feature becomes more evident for the sample with 100 mol% of zinc (R = 1), where no crystals melting is observed. Therefore, the disappearance of melting peaks observed through DSC is associated with high-melting soaps formation.

The crystalline structure of these samples was finally recognized using powder X-ray diffraction (XRD). The normalized spectrum in Figure 2b shows the above mixture of glutaric acid with 10 mol% of Zn(OAc) (R = 0.1). Evidently, the characteristic peaks of GluA decrease with the introduction of zinc, while new signals become detectable. The newly appeared peaks correspond to crystalline zinc glutarate[30] with a crystal size of about 0.1 µm, as given by the Scherrer formula (Figure S2 and Table S2).

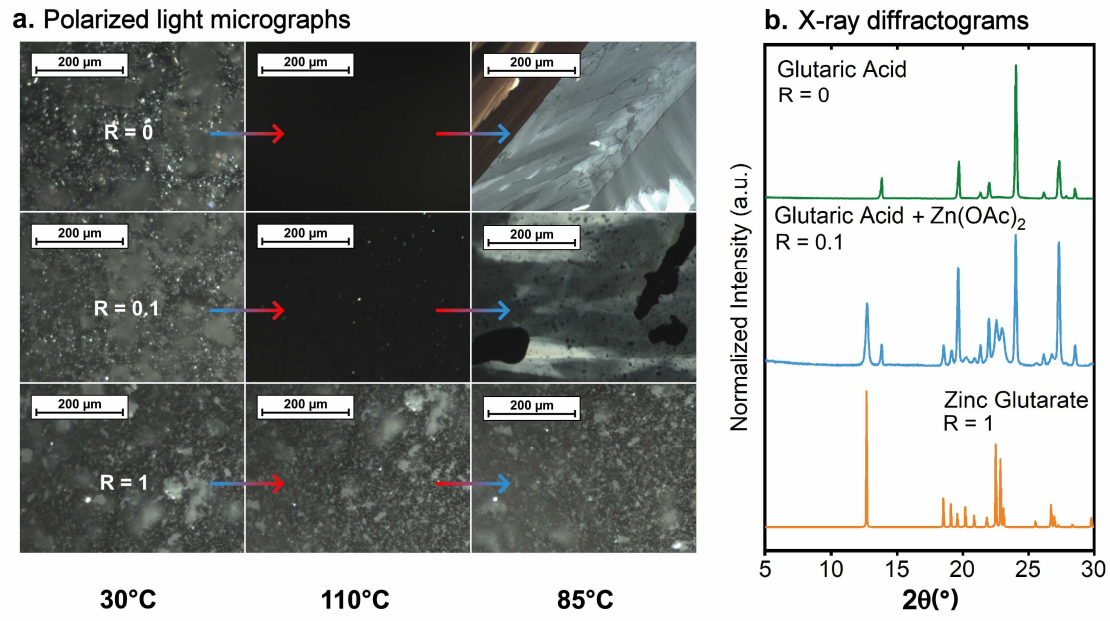


**Figure 2**: (a) POM images showing the melting behaviour of GluA (top), GluA + 10 mol% of $Zn(OAc)_2$ (R = 0.1, middle) and GluA + 100 mol% of $Zn(OAc)_2$ (R = 1, bottom) ; (b) Stack of X-ray diffraction spectra showing the spontaneous formation of metal soaps when mixing GluA and $Zn(OAc)_2$. Pure glutaric acid (green), mixture of glutaric acid with 10 mol% of $Zn(OAc)_2$ (blue) and zinc glutarate (orange, calculated from ref 30 data).

**Effect of Metal Soaps on Model Reactive Mixtures.** As second step of this study, model formulations containing a carboxylic acid, a Zn(II) catalyst and a diepoxide were prepared (Table S3). Figure 3 shows cure monitoring data for two different diacids: glutaric acid (GluA, $T_m$ = 98°C) and Pripol 1009 (FatA, a non-crystallizable dicarboxylic acid). Curing was performed at 145°C, with Zn at Zn(II)/COOH = 0.1 ratio and without zinc. For these experiments, a non-aromatic epoxy monomer, cyclohexanedimethanol diglycidyl ether (CHDE), was selected to leave clear the 1500–1850 $cm^{-1}$ absorption range. The regions of interest of infra-red spectra are shown in Figure 3b, 3c and S4. At the beginning of the experiments, two carbonyl vibrations are already detected at $\overline{\nu} \approx 1701$ $cm^{-1}$ and $\overline{\nu} \approx 1730$ $cm^{-1}$. These respectively correspond to carboxylic acids, mutually H-bonded and H-bonded with an ethereous solvent (here, the epoxy resin plays the role of the solvent). This feature has already been encountered in previous works[40,44] and more detail can be found in the SI (Figure S3). Epoxide vibrations are visible at ≈ 910 $cm^{-1}$ and 831 $cm^{-1}$. Whenever Zn(II) is present, other peaks are also detected in the 1650–1500 $cm^{-1}$ range (Figure S4), attributable to vibrations of carboxylate anions. Overtime integration of the epoxide signal is plotted in Figure 3d and 3e.

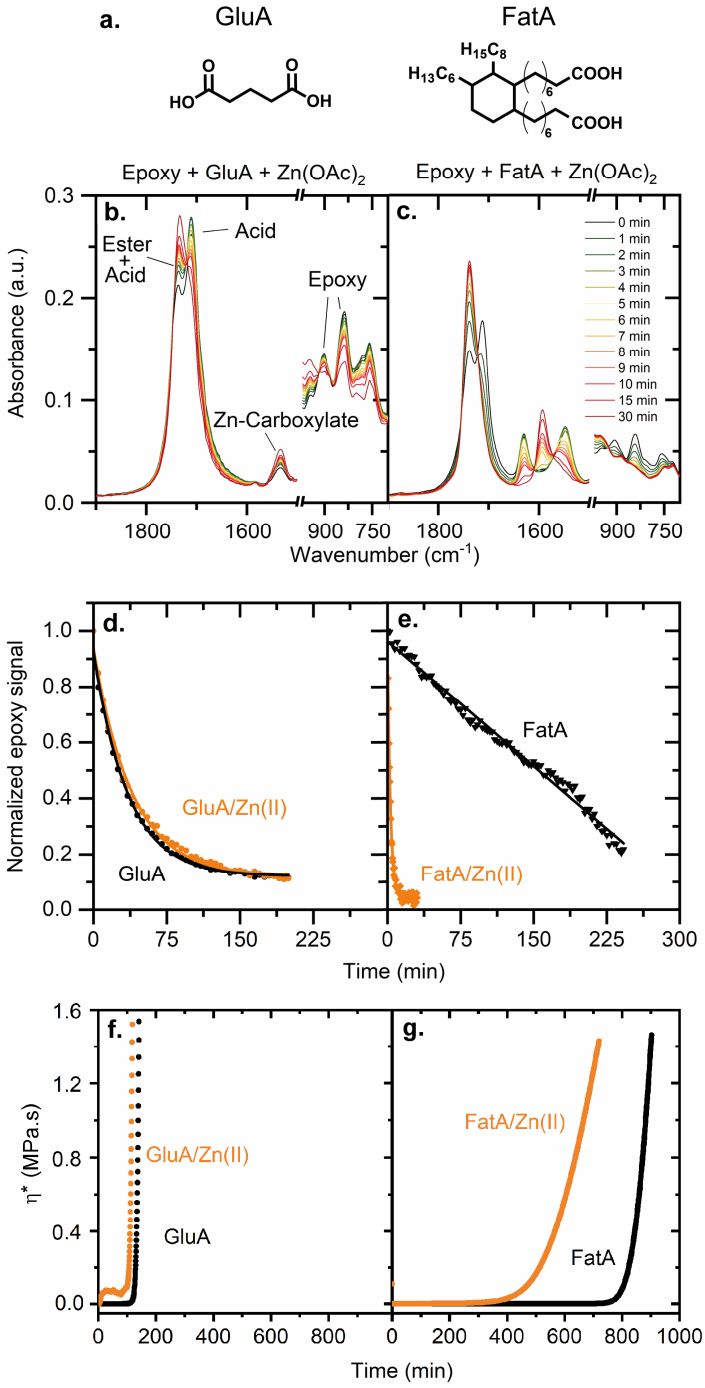


**Figure 3:** Chemical structure of the dicarboxylic acids (a) investigated in model reactive mixtures, using CHDE as epoxy precursor. IR monitoring of the reaction at 145°C: the carbonyl and epoxy peaks evolution is shown in (b) and (c); the normalized integration of the epoxy signal is reported in (d) and (e), and compared with reference systems without catalyst; the rheological monitoring of viscosity is reported in (f) and (g).

For the CHDE/GluA/Zn(II) system (Figure 3b), despite a clear reduction of epoxide and acid signals and appearance of ester peak at 1740 cm$^{-1}$, the carboxylate peak at 1530 cm$^{-1}$ did not

decrease over time and slightly increased instead. This indicates that the carboxylate salt formed at early stage of the reaction is not consumed during curing, supporting the picture of irreversible precipitation of the zinc soaps when processing with this rigid diacid monomer. In the case of the CHDE/FatA/Zn(II) system (Figure 3c), the carboxylate salt present at the beginning of the reaction shows two peaks at 1630 and 1548 $cm^{-1}$. These two peaks disappear after 30 minutes, and a new peak emerges at 1592 $cm^{-1}$, corresponding to zinc complexes where part of the bridging carboxylates are replaced by oxides or alkoxides.[45,46] In contrast to above zinc glutarate precipitates, which are infinite frameworks, these species are molecular entities involving a small number of zinc atoms that can be more efficiently dispersed in the reaction media. The distinct behaviour observed for GluA-Zn(II) and FatA-Zn(II) was found to impact the overall epoxy-acid addition kinetics, as shown in Figures 3d and 3e. The reaction rate constants $k_{add}$ were determined from first-order fits are reported in Table S3. Specifically, when the dicarboxylic acid is GluA (Figure 3d), the decay of the epoxide signal is not accelerated by the presence of Zn, consistent with the fact this metal is entirely converted to insoluble zinc glutarate. In contrast, in the case of FatA (Figure 3e), epoxy decay is initially slower than with GluA – and this is accounted for by the dilution effect brought by long fatty chains – but the addition of Zn considerably accelerates the reaction, in line with homogeneous dissolution of Zn ions and formation of efficient catalytic species in their solvation shell, as inferred by IR spectroscopy.

This precipitation issue was not observed in early works on vitrimers, were vegetable oil fatty diacids like FatA were systematically used.[1-3] The ligand exchange of FatA with zinc acetate leads to a crumbly solid with a melting temperature of ~ 50°C (Figure S5). This lower melting point – compared to linear dicarboxylic acid - is clearly related to the branched structure of the ligand, which hinders the formation of ordered crystalline lamellae with high thermal stability, a unique feature that enabled the preparation of well-behaved vitrimers in reference 1 and many related works.

Parallel to IR analysis, rheological cure monitoring was also carried out. (Figure 3f, g). All compositions eventually reach the gel point but with significantly different gel times (Figure S6). If considering solely the epoxy-acid addition from bifunctional monomers, gelation is not supposed to occur unless the involvement of another reaction like transesterification, etherification, epoxide ring-opening homopolymerization (and/or oxidative couplings, this last frequently reported for FatA[47]). CHDE/GluA and CHDE/GluA/Zn(II) systems exhibit similar complex viscosity increase $\eta^*$, as well as gelation times $t_{gel}$ and moduli $G'$ and $G''$ values. In this case, gelation occurs at relatively low epoxy conversion, suggesting a chain-

growth rather than step-growth polymerization mechanism[48] thus identifying epoxide homopolymerization as the leading reaction responsible for networks formation. For CHDE/FatA and CHDE/FatA/Zn(II) samples, gelation occurs well after complete consumption of the epoxy functions. Here, the observed difference between CHDE/FatA and CHDE/FatA/Zn(II) is clearly due to the involvement of Zn(II) catalyzed transesterification in the second system.

**Strategy to Avoid Soap Crystallization.** Enlarging the choice or reagents beyond the family of branched carboxylic acids is desirable to modulate the properties of the final material, such as achieving higher $T_g$ while keeping vitrimer-like behaviour. Here, we propose a strategy to avoid precipitation of metal soaps during vitrimer formulation. The concept, illustrated in Figure 4 and detailed in Scheme S2, involves first the synthesis of a COOH-terminated branched prepolymer, BranchA, whose structure is sufficiently disordered to prevent the crystallization of the metal soaps. An epoxy resin, PPGEF, is first reacted with a large excess of the dicarboxylic acid GluA in such a way gelation is avoided and oligomers with COOH terminals are formed (Figure 4a). Subsequently, the unreacted GluA is washed out and the obtained branched carboxylic acid BranchA, mixed with a stoichiometric amount of PPGEF, together with the $Zn(acac)_2$ catalyst to obtain a network. The details of the preparation are reported in SI and $^{1}H$ and $^{13}C$ NMR spectra of starting and final products are visible in Figures S7 to S12. SEC of PPGEF and BranchA are shown in Figure S13.

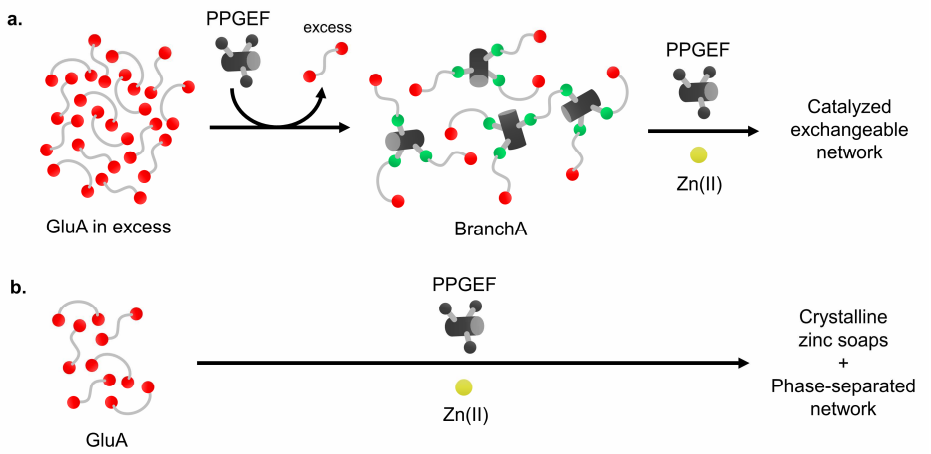


**Figure 4**: Strategy (a) to avoid precipitation of metal soaps during vitrimer preparation, with isolation of a non-crystallizable branched prepolymer used as network precursor in a second step. Classic workup (b) where zinc and acids get consumed in crystalline metal soap precipitates.

Different networks, described in Table S4, were obtained from PPGEF and different diacid/catalyst combinations using the classic workup with a curing step at 145°C. Vitrimer properties were studied through stress relaxation experiments in torsional rheology. The results are summarized in Table S5. For PPGEF/FatA/Zn(II), experiments shown in Figure S14 reveal efficient stress relaxation and an activation energy $E_a$ = 154 kJ/mol, consistent with previous reports. In contrast, for PPGEF/GluA/Zn(II), the network hardly relaxes the stress (Figure 5b) with negligible temperature effect. This behaviour is highlighted by the difficulty in mechanical reprocessing of the sample (Figure 5c). On the other hand, PPGEF/BranchA/Zn(II) presents an overall same composition as PPGEF/GluA/Zn(II), but stress relaxation experiments show strikingly different behaviour. In this case, the relaxation is complete and an $E_a$ = 78 kJ/mol is measured (Figure S15) and the material can be properly reprocessed: compression molding yields an homogeneous slab (Figure 5c) with similar modulus and stress relaxation properties as the original sample (Figure S16). After rheological experiments, samples were ground and investigated in XRD. The diffractograms are presented in insets of Figure 5b: the 002 peak of zinc glutarate is detected in PPGEF/GluA/Zn(II), while PPGEF/BranchA/Zn(II) is amorphous. This serves as final proof that catalytic activity towards transesterification is directly linked to metal homogenization and diffusion into the polymer matrix, and that precipitation of Zn(II) or other metal soaps severely compromises achievement of vitrimer properties.

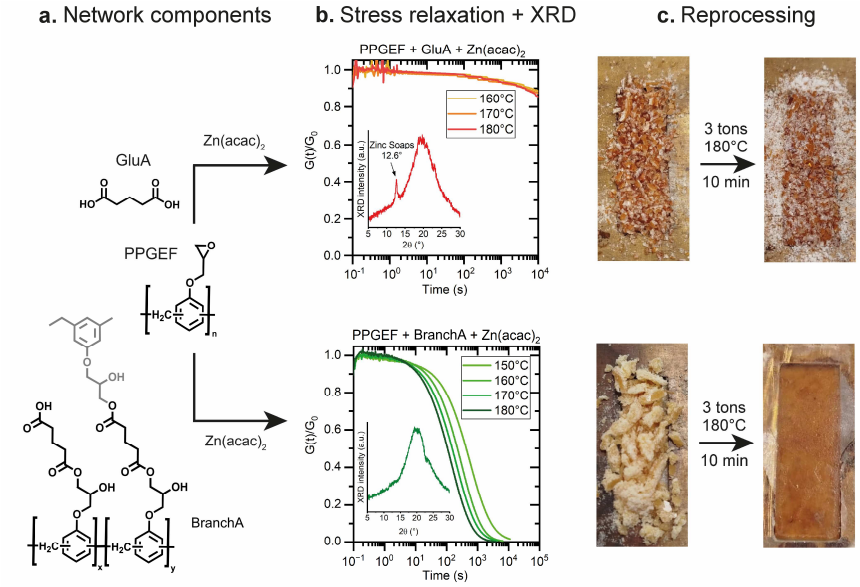


**Figure 5**: (a) Vitrimer networks with identical gross composition but cross-linked through the two different strategies of Figure 4. (b) Stress-relaxation and XRD of networks obtained from GluA (top) and BranchA (bottom). (c) Reprocessing of cured networks through grinding and recompression at 180°C.

**Catalyst Phase-Separation and Network Morphology.** A similar negative effect of metal-carboxylate interaction on catalytic performance was already reported in polyester based vitrimers, comprised of an amorphous polymer backbone with multiple COOH side groups, partially ionized with Zn(II) counterions.[49] In that case, crystallization was not observed, probably due to the lack of chain regularity, but aggregation of zinc ions took place upon annealing, through formation of an ionomer. As a result, the presence of big size clusters, with a large scattering signal around $q$ = 0.05 $Å^{-1}$ correlated with a slowed stress relaxation in annealed samples.[49]

To detect such mesoscopic phase-separation, X-ray scattering (SAXS-WAXS) experiments have been carried out covering the whole $q = 10^{-3}$ to 2 $Å^{-1}$ wavevector range. The results are plotted in Figure 6. Both formulations indeed show a shoulder in the SAXS range. Fitting with the same shape-independent model[50] for both PPGEF/GluA/Zn(II) and PPGEF/BranchA/Zn(II) cases allowed to measure correlations lengths of $\xi \approx 160$ Å and $\xi \approx 20$ Å respectively. Considering that this length is an estimate of the distance between zinc aggregates makes it possible to evaluate the aggregation number, $N_{agg}$ from its molar concentration. For PPGEF/GluA/Zn(II) the calculation (detailed in SI) gives $N_{agg} > 800$, confirming that Zn(II) is non evenly distributed in this sample. In the WAXS region, the same sample shows a series of Bragg peaks, whose broadening gives an estimated crystal size around 250 Å, in the same range as the above measurement. Thus aggregation of zinc atoms in this sample can be accounted for by precipitation rather formation of an ionomer. For PPGEF/BranchA/Zn(II) the estimated aggregation number $N_{agg}$ is less than 5 and Bragg peaks are hardly detected in the WAXS region, supporting formation of discrete aggregates containing a small number of metal atoms[45,46] and therefore a more homogeneous distribution of the metal inside the network.

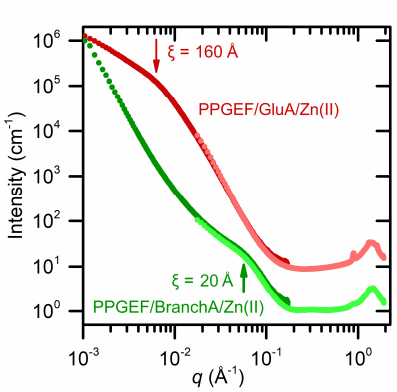


**Figure 6:** SAXS-WAXS patterns of PPGEF/GluA/Zn(II) (shifted one decade upwards for clarity) and PPGEF/BranchA/Zn(II) (bottom). The ticks indicates the correlation-length, ξ given by shape independent fitting.

The homogenization of the metal catalyst is also reflected by the thermomechanical spectra of the different network. Dynamic mechanical analysis (DMA) of PPGEF/BranchA/Zn(II) and PPGEF/GluA/Zn(II), together with its uncatalyzed counterpart PPGEF/GluA are presented in Figure 7 and values are summarized in Table S6. PPGEF/BranchA/Zn(II) and PPGEF/GluA have the same storage modulus *G'* and glass transition $T_g$, indicating that direct copolymerization or preparation through the BranchA precursor give rise to the same network connectivity. In contrast, the significantly higher *G'* and $T_g$ values of PPGEF/GluA/Zn(II) as well as the broadening and splitting of the tan(δ) peak indicate presence of rigid crystalline inclusions and phase separation of GluA-rich and GluA-poor regions with onset of side reactions such as epoxide homopolymerization in the latter. This last point is also confirmed by measurements of an overall lower swelling ratio in a good solvent, indicating denser crosslinking (Table S6).

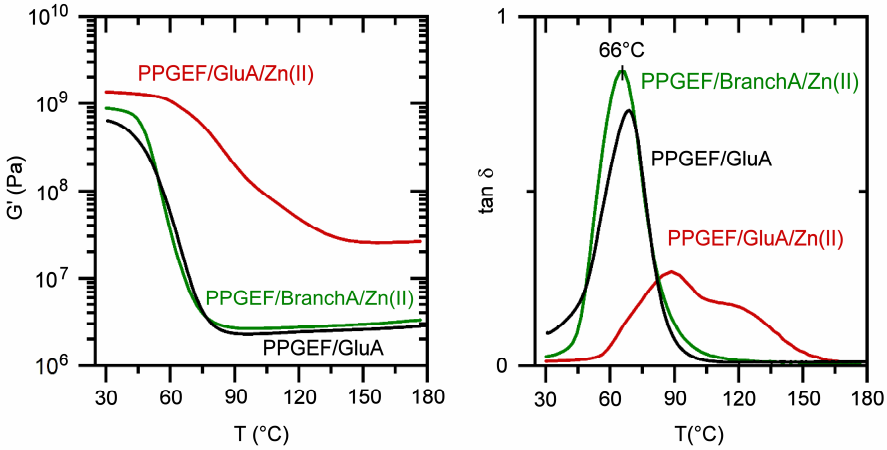


**Figure 7:** Temperature dependence of storage modulus (left) and loss factor (right) of PPGEF-based networks (measurements by DMA at 1 Hz).

**Possible Organometallic Alternatives.** Recently, Grésil and co-workers used butyl stannanoic acid (BuSnOOH) in epoxy-acid vitrimer formulations.[6] We observed that BuSnOOH remains soluble up to 5 mol% into GluA (Figure S5), and that the epoxy-acid addition is catalysed in CHDE-based formulations (Figure S17). For comparison with the strategy presented above, the PPGEF/GluA/BuSnOOH network (5 mol% catalyst) has been investigated. Rheological experiments revealed almost complete stress-relaxation, up to 95%, and an activation energy of about 130 kJ/mol (Figure S18) albeit with an about 10 times slower relaxation rate. In this case, the proper activity of the metal catalyst is likely related to the specific structure of this organotin molecule, wherein the metal shows an electron vacancy but no net positive charge.[51,52] Sn is in the same period as C and Si and can form covalent compounds that are formally similar to purely organic molecules but contrary to C and Si, organic Sn can accommodate multiple oxygen atoms in the next neighborhood, thus facilitating the interchange of alkyl fragments between coordinated ester groups.[53] Our experiments indicate that tin is not exchangeable in this molecule and thus does not precipitate in crystalline soaps.

## CONCLUSION

In brief, we illustrated an obstacle in the road of producing high $T_g$ metal-catalyzed vitrimers from acid and epoxy monomers. The favorite procedure where all reagents are mixed in the molten state is not applicable when using short chain rigid diacids as it causes precipitation of crystalline, highly thermally stable metal soaps; this phenomenon occurs across a variety of diacid and metals. Taking a novolac epoxy resin, glutaric acid and zinc as a model system, we showed that crystallization of zinc soaps makes the metal no longer available for catalysis. To circumvent this issue, we devised a non-crystallizable branched polyacid made from the same monomers. We compared the network made in one pot from the monomers with the network made from the branched intermediate. With the same gross composition, we obtained strikingly different results: On one hand, no discernible vitrimer properties and presence of crystalline inclusions; on the other fast relaxation (50% of stress relaxed in about 100 s) and evenly distributed zinc complexes.

Once this precipitation problem is under control, it becomes possible to broaden the range of usable monomers but also to study the role of the catalyst concentration in the network, discriminating the catalytic activity of the single atom on the exchange reaction from its tendency to precipitate or to form ionomer-type aggregates. Notwithstanding the development

of alternative catalytic solutions, we anticipate that the strategies hereby discussed will contribute to strengthen the design principles and processing methods for metal-catalyzed vitrimers, particularly for applications where the thermal stability of the catalyst is a major concern.

**Supporting Information:** Analysis of crystal structures, Dynamic scanning calorimetry, infrared spectroscopy, X-ray diffraction analysis, pictures showing metal soap precipitation and melting, rheological monitoring of curing experiments, IR, $^{1}H$ and $^{13}C$ NMR and SEC of synthesized products, stress relaxation and torsional rheology of networks, aggregation number estimation.

**Acknowledgements:** The research leading to these results has received funding from the Vitrimat project of the European Union's Horizon 2020 research and innovation program under the Marie Sklodowska-Curie Grant agreement No 860911. The European Space Agency (ESA contract 4000128430/19/NL/KML/afm) is thanked for financial support. I. R. acknowledges financial support from France 2030 under the reference ANR-22-PETA-0006 (Smart4Module Project – PEPR TASE). Huntsman is thanked for the gift of Epalloy resin samples. Paolo Edera is acknowledged for validation of the torsional rheology protocol. Yurii Dovgaliuk is warmly thanked for his help in X-ray diffraction experiments. We acknowledge SOLEIL for provision of synchrotron radiation facilities allocated to the GDR2019 CNRS/INRAE. We thank Javier Perez for assistance in using beamline SWING.

## References

[1] Montarnal, D.; Capelot, M.; Tournilhac, F.; Leibler, L. Silica-Like Malleable Materials from Permanent Organic Networks. *Science* **2011**, *334*, 965−968.
[2] Capelot, M.; Montarnal, D.; Tournilhac, F.; Leibler, L. Metal-Catalyzed Transesterification for Healing and Assembling of Thermosets. *J. Am. Chem. Soc*. **2012**, *134*, 7664–7667.
[3] Capelot, M.; Unterlass, M., M.; Tournilhac, F.; Leibler, L. Catalytic Control of the Vitrimer Glass Transition. *ACS Macro Lett*. **2012**, *1*, 789–792.
[4] Brutman, J. P.; Delgado, P. A.; Hillmyer, M. A. Polylactide Vitrimers. *ACS Macro Lett.* **2014**, *3*, 607−610.
[5] Liu, W.; Schmidt, D. F.; Reynaud, E. Catalyst Selection, Creep, and Stress Relaxation in High-Performance Epoxy Vitrimers. *Ind. Eng. Chem. Res.* **2017**, *56*, 2667−2672.
[6] Tangthana-umrung, K.; Poutrel, Q. A.; Gresil, M. Epoxy Homopolymerization as a Tool to Tune the Thermo-Mechanical Properties and Fracture Toughness of Vitrimers. *Macromolecules* **2021**, *54*,8393−8406.
[7] Altuna, F. I.; Hoppe, C. E.; Williams, R. J. J. Epoxy Vitrimers with a Covalently Bonded Tertiary Amine as Catalyst of the Transesterification Reaction. *Eur. Polym.J*. **2019**, *113*, 297−304.
[8] Hayashi, M. Dominant Factor of Bond-Exchange Rate for Catalyst-Free Polyester Vitrimers with Internal Tertiary Amine Moieties. *ACS Appl. Polym. Mater*. **2020**, *2*, 5365−5370.

[9] Delahaye, M.; Winne, J. M.; Du Prez, F. E. Internal Catalysis in Covalent Adaptable Networks: Phthalate Monoester Transesterification As a Versatile Dynamic Cross-Linking Chemistry. *J. Am. Chem.Soc*. **2019**, *141*, 15277−15287.

[10] Bakkali-Hassani, C.; Edera, P.; Langenbach, J.; Poutrel, Q.-A.; Norvez, S.; Gresil, M.; Epoxy Vitrimer Materials by Lipase-Catalyzed Network Formation and Exchange Reactions. *ACS Macro Lett.* **2023**, *12*, 338–343.

[11] Demongeot, A.; Groote, R.; Goossens, H.; Hoeks, T.; Tournilhac, F.; Leibler, L. Cross-linking of poly (butylene terephthalate) by reactive extrusion using Zn (II) epoxy-vitrimer chemistry. *Macromolecules* **2017**, *50*, 6117−6127.

[12] Demongeot, A.; Mougnier, S. J.; Okada, S.; Soulié-Ziakovic, C.; Tournilhac, F. Coordination and Catalysis of $Zn^{2+}$ in Epoxy-Based Vitrimers. *Polym. Chem*. **2016**, *7*, 4486−4493.

[13] Taylor, R. A.; Ellis, H. A. Anhydrous polymeric zinc(II) pentanoate. *Acta Cryst.* **2008**, E64, m895, https://doi.org/10.1107/S1600536808008283

[14] Torruco Baca, B.; del Castillo, L. F.; Vera-Cruz, P.; Toscano, R.A. Rodríguez-Hernández, J.; Balmaseda, J. Synthesis, characterization, and crystal structure of two zinc linear dicarboxylates. *Powder Diffraction* **2016**, *31*, 229–232.

[15] Miles, D., G.; Ross, J. Mixed Calcium Salts of Soaps and Anionic Detergents. *Ind. Eng. Chem.* **1943**, *35*, 1298–1301.

[16]Akanni M. S.; Oko, E., K.; Borrows, H., D.; Ellis, H., A. The valent thermal behavior of divalent and valent metal soaps, a review. *Thermochim. Acta* **1992**, *208*, 1−41.

[17] Ordonez, E.; Twilley, J. Clarifying the Haze: Efflorescence on Works of Art. *Anal. Chem.* **1997**, *69*, 416A–422A.

[18] Wakabayashi, K.; Register, R.A. Ethylene/(meth)acrylic acid ionomers plasticized and reinforced by metal soaps. *Polymer* **2006**, *47*, 2874–2883.

[19] Lévai, G.; Ocskay, G.; Nyitrai, Z.; Meszlényi, G. Kinetics of the stabilizing effect of calcium and zinc stearates in the thermal degradation of PVC: Part I, *Polym. Degradat. Stability* **1989**, *25*, 61.

[20] Mishra, S.; Daniele, S.; Hubert-Pfalzgraf, L.G.; Metal 2-ethylhexanoates and related compounds as useful precursors in materials science, *Chem. Soc. Rev.* **2007,** *36*, 1770.

[21] Osmond, G.; Boon, J. J.; Puskar, L.; Drennan, J. Metal Stearate Distributions in Modern Artists' Oil Paints: Surface and Cross-Sectional Investigation of Reference Paint Films Using Conventional and Synchrotron Infrared Microspectroscopy. *Appl. Spectrosc.* **2012**, *66*, 1136–1144.

[22] Hermans, J.; Keune, K.; van Loon, A.; Iedema, P. D. The crystallization of metal soaps and fatty acids in oil paint model systems. *Phys. Chem. Chem. Phys*. **2016**, *18*, 10896–10905.

[23] Schuchardt, U.; Sercheli, R.; Vargas, R., M. Transesterification of Vegetable Oils: a Review. *J.Braz.Chem.Soc.* **1998**, *9*, 199-210.

[24] Catalano, J.; Murphy, A.; Yao Y.; Yap, G. P. A.; Zumbulyadis, N.; Centeno, S., A.; Dybowski, C. Coordination geometry of lead carboxylates – spectroscopic and crystallographic evidence. *Dalton Trans*. **2015**, 44, 2340–2347.

[25] Barman, S.; Vasudevan, S. Melting of Saturated Fatty Acid Zinc Soaps. *J. Phys. Chem. B* **2006**, *110*, 22407-22414.

[26] Ishioka, T.; Maeda, K.; Watanabe, I.; Kawauchi, S.; Harada, M. Infrared and XAFS study on structure and transition behavior of zinc stearate. *Spectrochimica Acta Part A* **2000**, *56*, 1731 – 1737.

[27] Hermans J.; Helwig K. The Identification of Multiple Crystalline Zinc Soap Structures Using Infrared Spectroscopy. *Applied Spectroscopy* **2020**, *74*, 1505-1514.

[28] Reinoso, D., M.; Damiani, D., E.; Tonetto, G., M. Zinc carboxylic salts used as catalyst in the biodiesel synthesis by esterification and transesterification: Study of the stability in the reaction medium. *Applied Catalysis A: General* **2012**, *449*, 88–95.

[29] Tamames-Tabar, C.; Imbuluzqueta, E.; Guillou, N.; Serre, C.; Miller, S. R.; Elkaïm, E.; Horcajada, P.; Blanco-Prieto, M., J. A Zn azelate MOF: combining antibacterial effect. *CrystEngComm* **2015**, *17*, 456.

[30] Zheng, Y.Q.; Lin, J.-L.; Zhang, H.-L. Crystal structure of zinc glutarate, $Zn(C_5H_6O_4)$. *Zeitschrift für Kristallographie - New Crystal Structures* **2000**, *215*, 535-536.

[31] Zheng, Y. Q.; Lin, J. L.; New 1D and 2D metal oxygen connectivities in Cu(II) succinato and glutarato coordination polymers: $[Cu_3(H_2O)_2(OH)_2(C_4H_4O_4)_2].4H_2O$, $[Cu_4(H_2O)_2(OH)_4(C_4H_4O_4)_2].5H_2O$ and $[Cu_5(OH)_6(C_5H_6O_4)_2].4H_2O$. *J. Coord. Chem.* **2008**, *21*, 3420-3437.

[32] Pan, J.; Zhang, G.; Zheng, Y.; Lin, J.; Xu, Z. Growth and characterization of a novel nonlinear optical crystal zinc succinate, Zn(C4H4O4). *Journal of Crystal Growth* **2007**, *308*, 89–92.

[33] Hamel, C. M.; Kuang, X.; Chen., K.; Qi, H., J. Reaction-diffusion model for thermosetting polymer dissolution through exchange reactions assisted by small-molecule solvents. *Macromolecules* **2019**, *52*, 3636-3645.

[34] Shi, Q.; Yu, K.; Dunn, M. L.; Wang, T.; Qi, H., J. Solvent assisted pressure-free surgace welding and reprocessing of malleable epoxy polymers. *Macromolecules* **2016**, *49*, 5527-5537.

[35] Legrand, A.; Soulié-Ziakovic, C. Silica-epoxy vitrimer nanocomposites. *Macromolecules* **2016**, *49*, 5893-5902

[36] Chen, J.; Huang, H.; Fan, J.; Wang, Y.; Yu, J.; Zhu, J.; Hu, Z. Vitrimer Chemistry Assisted Fabrication of Aligned, Healable, and Recyclable Graphene/Epoxy Composites. *Front. Chem.* **2019**, *7*, 632.

[37] Zhang, S.; Liu, T.; Hao, C.; Wang, L.; Han, J.; Liu, H.; Zhang, J. Preparation of a lignin-based vitrimer material and its potential use for recoverable adhesives. *Green Chem* **2018**, *20*, 2995–3000.

[38] Hayashi, M.; Yano, R.; Takasu, A. Synthesis of amorphous low tg polyesters with multiple COOH side groups and their utilization for elastomeric vitrimers based on post-polymerization cross-linking. *Polym Chem* **2019**, *10*, 2047–2056.

[39] Chappuis, S.; Edera, P.; Cloitre, M.; Tournilhac, F. Enriching an Exchangeable Network with One of Its Components: The Key to High-Tg Epoxy Vitrimers with Accelerated Relaxation. *Macromolecules* **2022**, *55*, 6982−6991.

[40] Poutrel, Q., A.; Blaker, J., J.; Soutis, C., Tournilhac, F.; Gresil, M. Dicarboxylic acid-epoxy vitrimers: influence of the off-stoichiometric acid content on cure reactions and thermo-mechanical properties. *Polym. Chem.*, **2020**, *11*, 5327–5338.

[41] Arano, F., M.; Casado, U.; Zapata, I.; Rivera, F., J.; Churruca, M., J. Altuna, F., I.; Rodríguez, E., S.; Hoppe, C., E.; Williams, R., J., J. Self-Healing of Microcracks and Scratches in a Carbon-Fiber Reinforced Epoxy Vitrimer by Conventional or Remote Heating, *ACS Appl. Mater. Interfaces*, **2024**, ASAP, DOI: 10.1021/acsami.4c18025.

[42] Poutrel Q., A.; Retailleau, I.; Lafont, U.; Damiano, O.; Tournilhac, F.; Thermolatent Heterogeneous Epoxy–Acid Formulation for the Manufacture of Preimpregnated Sheets and Composites with Vitrimer Properties *ACS Appl. Polym. Mater.* **2023**, *5*, 6095–6106.

[43] Doucet M. et al. SasView Version 4.2.2, Zenodo, DOI:10.5281/zenodo.2652478

[44] Cazares-Cortes, E.; Baker, B.C.; Nishimori,K.; Ouchi, M.; Tournilhac, F. Polymethacrylic Acid Shows Thermoresponsivity in an Organic Solvent. *Macromolecules*, **2019**, *52*, 5995−6004.

[45] Hermans, J. J.; Baij, L.; Koenis, M.; Keune, K.; Iedema, P. D.; Woutersen, S. 2D-IR Spectroscopy for Oil Paint Conservation: Elucidating the Water-Sensitive Structure of Zinc Carboxylate Clusters in Ionomers. *Sci. Adv.*, **2019**, *5*.

[46] Francis, L. F.; Payne, D. A.; Wilson, S. R. Crystal Structure of a New Lead Zinc Acetate Alkoxide, Pb2Zn2(C2H3O2)4(C3H7O2)4. *Chem. Mater.* **1990**, *2*, 645–647.

[47] Kerenkan, A., E.; Béland, F.; Do, T.-O. Chemically catalyzed oxidative cleavage of unsaturated fatty acids and their derivatives into valuable products for industrial applications: a review and perspective. *Catal. Sci. Technol.*, **2016**, *6*, 971.

[48] Vidil, T.; Tournilhac, F. Supramolecular Control of Propagation in Cationic Polymerization of Room Temperature Curable Epoxy Compositions Macromolecules, **2013**, *46*, 9240-9248.

[49] Hayashi, M.; Obara, H.; Miwa, Y. Design and basic properties of polyester vitrimers combined with an ionomer concept, *Mol. Syst. Des. Eng.* **2021**, *6*, 234–241

[50] Hammouda, B.; Ho, D.L.; Kline, S.R. Insight into Clustering in Poly(ethylene oxide) Solutions, *Macromolecules* **2004**, *37* 6932-6937.

[51] Ingham, R., K.; Rosenberg, S. D.; Gilman, H. Organotin Compounds. *Chem. Rev.* **1960**, *60*, 459-539.

[52] Wardell, J.L. Formation and cleavage of the tin—carbon bond. In *Chemistry of Tin*, Springer, 1998. https://doi.org/10.1007/978-94-011-4938-9_4.

[53] Wolzak, L.A.; Hermans, J.J.; de Vries, F.; van den Berg, K.J.; Reek, J.N.H.; Tromp, M.; Korstanje, T.J. Mechanistic elucidation of monoalkyltin(IV)-catalyzed esterification. *Catal. Sci. Technol.* **2021**, *11*, 3326-3332.